Lab on a Chip

RSC Publishing

PAPER

View Article Online
View Journal | View Issue

Cite this: *Lab Chip*, 2013, **13**, 3893

Cell patterning *via* diffraction-induced optoelectronic dielectrophoresis force on an organic photoconductive chip†

Shih-Mo Yang,[a] Sheng-Yang Tseng,[b] Hung-Po Chen,[c] Long Hsu[b] and Cheng-Hsien Liu*[c]

Received 18th March 2013,
Accepted 6th July 2013

DOI: 10.1039/c3lc50351h

www.rsc.org/loc

A laser diffraction-induced dielectrophoresis (DEP) phenomenon for the patterning and manipulation of individual HepG2 cells and polystyrene beads *via* positive/negative DEP forces is reported in this paper. The optoelectronic substrate was fabricated using an organic photoconductive material, TiOPc, *via* a spin-coating process on an indium tin oxide glass surface. A piece of square aperture array grid grating was utilized to transform the collimating He–Ne laser beam into the multi-spot diffraction pattern which forms the virtual electrodes as the TiOPc-coating surface was illuminated by the multi-spot diffraction light pattern. HepG2 cells were trapped at the spot centers and polystyrene beads were trapped within the dim region of the illuminated image. The simulation results of light-induced electric field and a Fresnel diffraction image illustrated the distribution of trapped microparticles. The HepG2 morphology change, adhesion, and growth during a 5-day culture period demonstrated the cell viability through our manipulation. The power density inducing DEP phenomena, the characteristics of the thin TiOPc coating layer, the operating ac voltage/frequency, the sandwiched medium, the temperature rise due to the ac electric fields and the illuminating patterns are discussed in this paper. This concept of utilizing laser diffraction images to generate virtual electrodes on our TiOPc-based optoelectronic DEP chip extends the applications of optoelectronic dielectrophoretic manipulation.

Introduction

The ability to manipulate cells and microparticles into a desired arrangement has benefits for biological investigations and applications such as microarrays,[1–3] tissue engineering,[4–7] and regenerative medicine.[5,8] The invention of optical tweezers[9,10] and the various developments of holographic optical tweezers[11,12] have established platforms to manipulate either single or multi-microparticles *via* an optical approach. The electrokinetic approach of dielectrophoresis (DEP) is able to trap single particles as well as arrange numerous microparticles over a large-area.[13–15] Wu *et al.* integrated optical flexibility and electronic manipulation to propose the concept of optoelectronic tweezers (OET).[16] Its growing developments have been utilized for various engineering and biological applications.[16–24]

However, several limitations exist in these designs for microparticle manipulations. For example, the requirement of high N.A. value lenses in optical tweezers limits the working distance for microparticle manipulations.[25,26] Next, a component of holographic optical tweezers such as spatial light modulator (SLM) or digital micromirror devices (DMD) is necessitated to align critically in the light path. The velocity of the microparticle is related to the digital operation speed because its speed is proportional to the projecting image.[26] Then, the traditional DEP designs which utilize the fixed metal electrodes for dielectrophoresis lack flexibility for the manipulation of individual cells.[16,23] Specific facilities and critical processes, such as plasma-enhanced chemical vapor deposition (PECVD),[16] ion implantation, reactive ion etching,[19] and a nitrogen-filled glove box,[27] are usually required to fabricate optoelectronic-tweezer chips. Biological researchers without a knowledge of MEMS (Micro-Electro-Mechanical Systems) have had limited use of this powerful optoelectronic device.

In this research, we demonstrated a microparticle patterning technique with a long working distance, a simple optical system, and an easy process for fabrication of the optoelectronic chip based on an organic photoconductive material. We utilized the single He–Ne laser beam passing through a square aperture array of grid grating to generate diffraction patterns

[a]*Department of Mechanical and Automation Engineering, Chinese University of Hong Kong, Hong Kong*
[b]*Department of Electrophysics, National Chiao-Tung University, Hsinchu, Taiwan 300, R.O.C.*
[c]*Department of Power Mechanical Engineering, National Tsing Hua University, Hsinchu, Taiwan 300, R O.C.. E-mail: liuch@pme.nthu.edu.tw; Tel: +886-3-5742496*

† Electronic supplementary information (ESI) available: videos showing the demonstration of diffraction-induced optoelectronic dielectrophoresis force for the patterning of cells and polystyrene beads. See DOI: 10.1039/c3lc50351h

and integrated this optical phenomenon into our TiOPc-based optoelectronic DEP chip to position HepG2 cells and polystyrene beads in a designed array. The chip design and system setup has several innovative features for the optoelectronic manipulation of microparticles. Firstly, utilizing the multi-spot diffraction pattern to trap particles could avoid the drawbacks of high N.A. value lenses and short working distance. The laser diffraction pattern (with a little defocussing) is able to induce charge assembled on the TiOPc-coating surface as virtual electrode spots. Next, comparing the SLM system setup, only a piece of grid-shape grating mask based on the Fraunhofer diffraction principle is needed to generate the multi-spot pattern. Mathematical simulation (Fourier transform) can be utilized to illustrate the spot distribution of diffraction images. The optical system, one grating mask and two lenses, requires no complex optical design and no programmable code to control the illuminating pattern. Then, with the features of optoelectronic DEP chip, the virtual electrode spots on the TiOPc surface corresponding different diffraction pattern are able to trap microparticles, cells and polystyrene beads. Using this method, masks can be designed to generate specific diffraction patterns, which can trap microparticles into a desired pattern. Finally, only a single process is needed to fabricate the TiOPc-based chip which greatly improves the convenience of this optoelectronic dielectrophoresis technology.[28] The simple fabrication process reported in this paper provides researchers without MEMS background the opportunity to utilize this powerful and promising optoelectronic tool.

Operation principle of TiOPc-based chip

TiOPc characteristics

Recent research in semiconductor laser technology has rapidly increased and been widely applied to laser printing, copier applications, and digital xerography.[29,30] Studies have utilized phthalocyanine pigments as electrophotographic sensitive components, due to their efficient absorption from the visible to infrared regions.[31,32] In many optoelectronic chips,[16] photoconductive amorphous silicon (a-Si) layer is the significant component because it allows the impedance to be modified *via* light illumination. From this perspective, TiOPc and a-Si have similar photosensitive characteristics while they are in the dark and under illumination. The application of TiOPc instead of a-Si to generate a virtual electrode is a feasible approach to simplify the complex fabrication process.[28] Therefore, a Y-type TiOPc material with excellent absorption properties in the 700–800 nm region has been selected as the photoconductive material to fabricate the optoelectronic dielectrophoresis chip in our research.[32,33]

Dielectrophoresis

Dielectrophoresis(DEP) is a phenomenon caused by the induced dipole of the polarizable particles in the solution under non-uniform electric fields.[13] Over the past decade around 2000 publications have addressed the status of DEP theory, the developed technology, and it numerous applications. Research fields including biosensors, cell therapeutics, drug discovery, medical diagnostics, microfluidics, nanoassembly, and particle filtration have attracted the attention of DEP applications.[7,13,34] Most publications on DEP illustrate an expression for the time-average DEP force,[14] F_{DEP}, acting on a spherical particle of radius r suspended in a medium of relative permittivity ε_m as

$$F_{\mathrm{DEP}} = 2\pi r^3 \varepsilon_m \mathrm{Re}[f_{\mathrm{CM}}(\omega)]\nabla E_{rms}^2 \quad (1)$$

Here, E_{rms} is the root mean square of the ac electric field and $f_{\mathrm{CM}}(\omega)$ is the Clausius-Mossotti factor,[14] given by

$$f_{\mathrm{CM}}(\omega) = \frac{(\varepsilon_p^* - \varepsilon_m^*)}{(\varepsilon_p^* + 2\varepsilon_m^*)} \quad (2)$$

$f_{\mathrm{CM}}(\omega)$ indicates that the force vector acting on the particle varies with the applied frequency and depends on the permittivity and conductivity of the particle and medium.[14] If $f_{\mathrm{CM}}(\omega) > 0$, the particle is attracted toward the regions of the large electric-field gradient, this is called positive DEP or positive OET in the field of optoelectronic applications.[16,20,35–37] On the contrary, if, $f_{\mathrm{CM}}(\omega) < 0$, the particle is repelled toward the region with minimum local electric-field gradient and this is named negative DEP or negative OET.[16,19,20,38–40] The DEP force could be simplified as

$$F_{\mathrm{DEP}} \propto \nabla E_{rms}^2 \quad (3)$$

In this article, cells suspended in low conductive DEP buffer are driven to the laser diffraction spots by positive OET force and polystyrene beads suspended in deionized (DI) water are repelled toward the dim region of illuminating pattern. According to the relationship of formula (3), the distribution of ∇E_{rms}^2 simulations presents the DEP force effect on the TiOPc chip.

Wave propagation processes

Fig. 1 shows a schematic diagram of our simple optical-spot-generation system, a square aperture array on the grating mask, and functions of light transformation. A grid-shape grating mask is placed on plane 1, (x_1,y_1), shown in Fig. 1(a). As a collimated He–Ne laser beam illuminates the mask and propagates to plane 2, (x_2,y_2), the intensity distribution is changed due to Fresnel diffraction and imaged onto plane 3, (x_3,y_3), which is the plane of the TiOPc coating surface, by a microscope with a 1/20 × magnification to fit the working area of the substrate.

The grid mask is an opaque screen with a transparent rectangular array, of width Δx and height Δy, respectively, and has the periods of ΔX and ΔY along the x_1 and $y_1$directions respectively, as illustrated in Fig. 1(b). The transmittance of the mask can be expressed as

$$t(x_1,y_1) = rect\left(\frac{x_1}{\Delta x}\right) rect\left(\frac{y_1}{\Delta y}\right) \otimes comb\left(\frac{x_1}{\Delta X}\right) comb\left(\frac{y_1}{\Delta Y}\right) \quad (4)$$

where : represents convolution operation, $comb(x)$ is the function given by

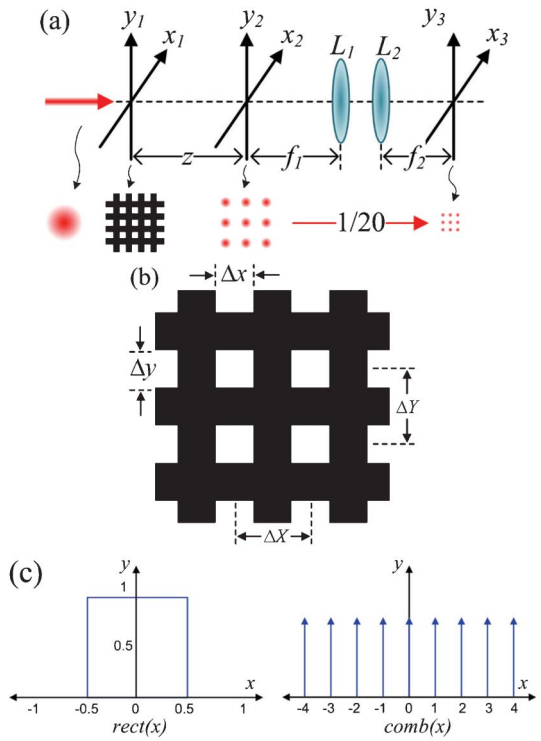

Fig. 1 (a) (x_1,y_1), (x_2,y_2) and (x_3,y_3) planes are defined as the specific position for the wave propagation process (b) Defined terms for the formula. Δx and Δy are the width and length of each square aperture, respectively. ΔX and ΔY are the distances of each square aperture center, respectively. (c) Rectangle function and comb function are applied to describe the optical transformation of the grid pattern.

$$comb(x) = \sum^{\infty} \delta(x-n) \tag{5}$$

$rect(x)$ is the function given by

$$rect(x) = \begin{cases} 1, |x| < \frac{1}{2} \\ \frac{1}{2}, |x| = \frac{1}{2} \\ 0, otherwise \end{cases} \tag{6}$$

These two functions are shown in Fig. 1(c). We assume that the field distribution of the incident laser beam is

$$E_{in}(x_1,y_1) = e^{-\left(\frac{x_1^2+y_1^2}{2w^2}\right)} \tag{7}$$

where x_1 and y_1 are the spatial coordinates of plane 1 and w is the beam radius of the laser beam. The field distribution, $E_Z(x_2,y_2)$, on plane 2 can be obtained by using Fresnel diffraction, that is

$$\begin{aligned} &E_z(x_2,y_2) \\ &= \frac{e^{jkz}}{j\lambda z} \iint E_{out}(x_1,y_1) e^{\left(\frac{jk}{2z}\right)\left((x_2-x_1)^2+(y_2-y_1)^2\right)} dx_1 dy_1 \\ &= \frac{e^{jkz}}{j\lambda z} \left[E_{out}(x_1,y_1) \otimes e^{\frac{jk}{2z}(x_1^2+y_1^2)} \right] \end{aligned} \tag{8}$$

where λ is the wavelength of the laser beam, $k = 2\pi/\lambda$ and z is the distance between plane 1 and plane 2. For a quick calculation of eqn (8), $E_Z(x_2,y_2)$ is often calculated in the frequency domain and is given by

$$E_z(x_2,y_2) = \frac{e^{jkz}}{j\lambda z} F^{-1}\left\{ F\{E_{out}(x_1,y_1)\} \cdot F\left\{ e^{\frac{jk}{2z}(x_1^2+y_1^2)} \right\} \right\} \tag{9}$$

From above equations we are able to calculate the observed diffraction pattern of intensity, $I_Z(x_2,y_2)$, in plane 2

$$\begin{aligned} I_z(x_2,y_2) &= |E_z(x_2,y_2)|^2 \\ &= \frac{1}{(\lambda z)^2} \left| F^{-1}\left\{ F\{E_{out}(x_1,y_1)\} \cdot F\left\{ e^{\frac{jk}{2z}(x_1^2+y_1^2)} \right\} \right\} \right|^2 \end{aligned} \tag{10}$$

The calculated results were simulated by the commercial software, Mathematica 7 (Wolfram Co., Ltd.).

The appropriate laser diffraction pattern illuminating on the TiOPc surface for the trapping of cells and polystyrene beads can be adjusted by tuning the distance, z, between the (x_2,y_2) and (x_3,y_3) planes.

The power density on the photoconductive substrate in the primary spots can be estimated *via* eqn (10). The value of the power density provides the evidence to revise the phenomenon of diffraction-induced optoelectronic dielectrophoresis. The detailed results will be discussed in the following simulation section.

Chip fabrication and system design

Optical system design

To project the laser diffraction spots onto the TiOPc surface, we design a grid-shape grating mask to generate the optical diffraction phenomenon. A two-dimension square aperture array was designed as shown in Fig. 1(b) with $\Delta x = \Delta y = 100$ μm and $\Delta X = \Delta Y = 200$ μm. The grating pattern was drawn with laser pattern generator (HIMT DWL_200) on a 200 mm × 200 mm quartz glass. When a He–Ne laser (NT62-715, 0.5 mW) beam passes through the grid-shaped grating mask, each single hollow square aperture is regarded as an individual laser source for wave propagation to generate a Fresnel diffraction image. To match the size of the target microparticles and the desired gap between microparticles, a pair of confocal lenses, lens 1 and lens 2, with a 10 mm and 200 mm focal length, respectively, were placed between the TiOPc-based chip and the grid-shaped grating mask. The original diffraction pattern was formed at the focal plane of lens 1,

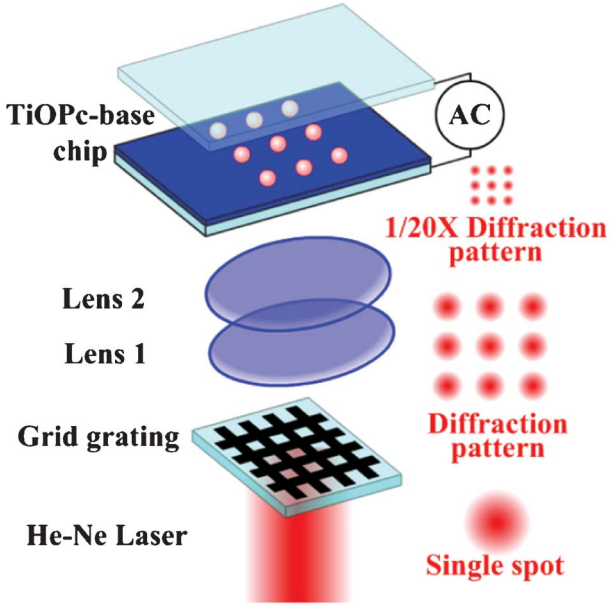

Fig. 2 The relative position of each optical element and the diffraction-induced optoelectronic dielectrophoresis chip. A single collimated He–Ne laser beam passes through a square aperture grid grating mask. A pair of lenses is utilized to minimise the laser diffraction pattern 1/20 × and to project it onto the surface of the TiOPc-coating substrate to form virtual electrode spots. A function generator provides the external ac voltage for the manipulation of cells/microparticles. The cells are patterned/trapped at the diffraction spots on the chip.

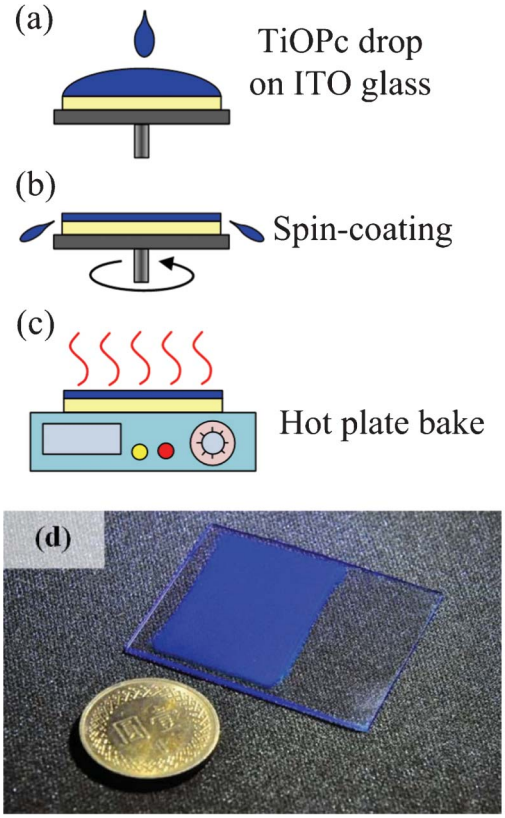

Fig. 3 (a) The TiOPc solution was dropped onto the ITO glass. (b) A spin-coating process was utilized to spread a thin TiOPc layer on the ITO glass substrate. (c) The substrate was baked to dry the organic solvent and harden the TiOPc structure. (d) TiOPc-coating ITO substrate. The pattern size of the TiOPc layer was modified by using alcohol to dissolve the organic photoconductive material.

(x_2,y_2). The TiOPc-coating substrate was placed at the focal plane of lens 2, (x_3,y_3) as shown in Fig. 1 (a). The red spots of differing sizes at the right side of Fig. 2 illustrate the cross-section of a collimated laser beam. The diffraction image was projected onto the focal plane of lens 1 and the TiOPc surface. We selected the bright 3 × 3 spots array at the center of diffraction image for the demonstration of cell patterning/trapping.

Chip fabrication and electric-field simulation

A 500 μl TiOPc droplet was placed on a 2.5 cm × 3 cm indium tin oxide (ITO) glass surface, spin-coated at 1500 rpm for 20 s to form a 200 nm thin layer, and baked at 130 °C for 30 min to dry the organic solvent to harden the TiOPc layer. The fabrication steps are illustrated in Fig. 3(a)–(c). The dried TiOPc layer cannot be dissolved in water, however an organic solvent such as an aqueous alcohol solution is able to dissolve it. Therefore, we used alcohol to modify the TiOPc pattern size for convenience as shown in Fig. 3(d).

The chip consists of a sandwich structure–a top transparent ITO layer, a buffer with suspended cells or microparticles, and a thin TiOPc layer coating on the bottom ITO glass, as shown in Fig. 4. The distance between the top ITO surface and bottom TiOPc-coating substrate was adjusted by the tape thickness which was 80–200 μm. The applied alternating current (ac) potential and frequency was controlled using a function generator (33120A, Agilent). Commercial simulation software CFD–ACE+ (CFDRC, Huntsville, AL) was utilized to depict the steady-state electric field which contributed to the diffraction-induced optoelectronic dielectrophoresis. The color distributed between the top cover and the bottom ITO substrate shows the simulation results for the root mean square of ac electric field (E^2) neighboring the diffraction-induced charged electrodes on the TiOPc-coating substrate. The yellow dotted lines illustrate the electric-field line paths.

According to the similar working principle of the OET,[19] the sandwiched liquid medium and organic photoconductive layer of TiOPc-based chip can be modeled as two electrically resistive elements connected in series as shown in Fig. 4.

Under the high-frequency operating conditions, (greater than 1 MHz), the impedance of TiOPc is dominated primarily by the resistance effect. The effect of the capacitance of the photoconductive layer could be ignored. Without light illumination, the TiOPc has a higher impedance than the medium and most of the voltage drops across the photoconductive layer. The electric-field distribution in liquid is uniform and no DEP effect is observed. As the light is projected onto the photoconductive layer, the TiOPc impedance within the illuminated region decreases. The charges pass through the TiOPc layer within the light pattern to be assembled as virtual electrodes on the substrate surface. Then, most of the voltage drops across the medium layer. Therefore,

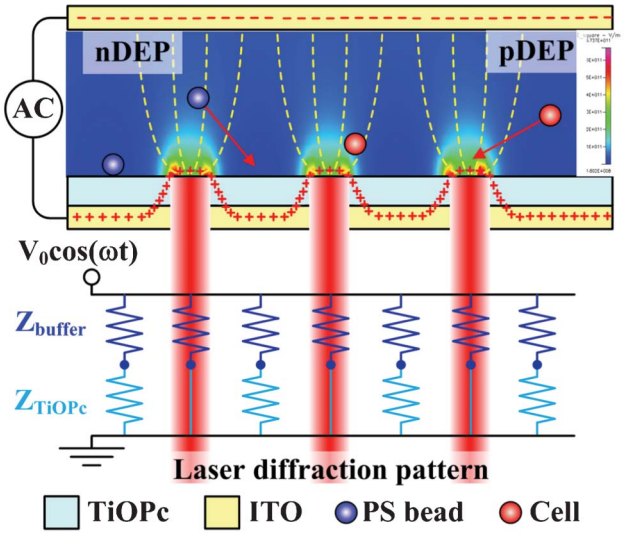

Fig. 4 The schematic diagram of DEP electric-field simulation and the relative alternating current bias model for the sandwiched liquid medium and the organic photoconductive layer. Without illumination, most of the voltage drops across the TiOPc layer. As the light is projected onto the photoconductive layer, its impedance is reduced and the charges pass through the TiOPc layer within the illuminating region to form a virtual electrode on the bottom substrate. Then, most voltage drops across the medium. The non-uniform electric field is generated *via* the large ITO electrode on the top cover and the small virtual electrode at the bottom. The yellow dotted lines illustrate the electric-field line. The color simulation reveals the ac electric-field (E^2) distribution which induces the DEP phenomenon. The positive DEP force attracts the HepG2 cell (red) toward the illuminating spot and the negative DEP force repels the polystyrene particle (blue) to the dim region of laser diffraction pattern.

the large ITO electrode on the top cover and the small virtual electrode at the bottom generate a non-uniform electric field to perform the DEP effect. Under the positive DEP operating conditions, the cell is attracted toward the strong electric-field region, the center of the illuminating spot. The polystyrene beads affected by the negative DEP force are repelled to the weak electric-field region, the dim area of laser diffraction pattern. By modifying the illuminating pattern, the TiOPc-based chip can be utilized to demonstrate the functions of the desired microparticle/cell patterning.

Results and discussion

Cell patterning/trapping *via* diffraction spots

To demonstrate the light-induced DEP phenomenon, the liver cells, HepG2, were used for cell trapping. HepG2 cells were harvested from subconfluent cultures by trypsin/EDTA (Sigma), suspended in a low conductivity DEP manipulation buffer (8.5% sucrose and 0.3% dextrose in distilled deionized water; conductivity, 10 mS m^{-1}), and pumped in, to be sandwiched between the top ITO glass and the bottom TiOPc-coating substrate. When the ac potential was applied and the laser diffraction pattern was projected onto the working region on the chip, the cells were attracted toward the strong electric-field location, the centers of the illuminating spots on the

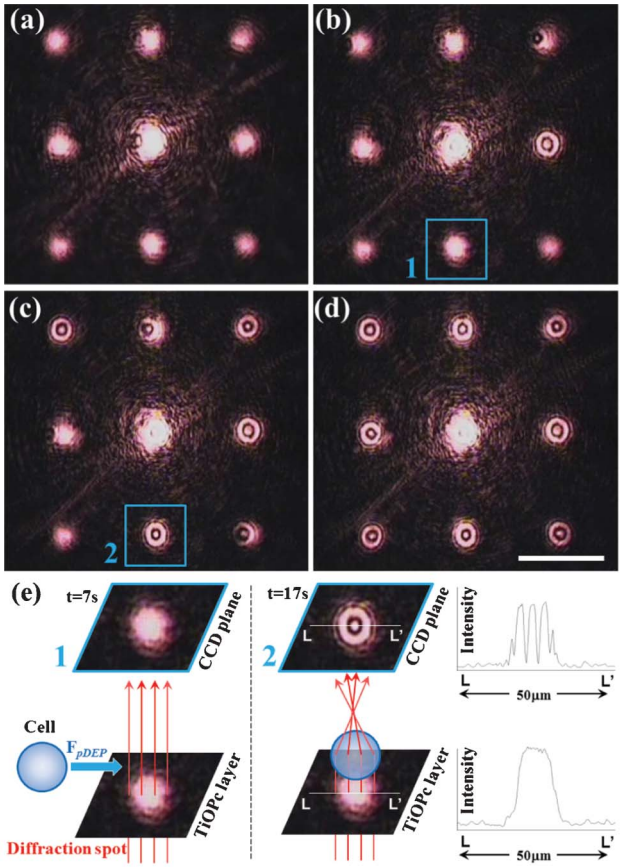

Fig. 5 (a)–(d) The laser diffraction pattern generates virtual electrode spots on the TiOPc substrate. Nine HepG2 cells are attracted toward each spot center due to the positive DEP force. (a), (b), (c) and (d) are recorded at 0, 7, 17 and 26 s, respectively. (e) The images on the TiOPc layer surface and the CCD plane and the related light intensity analyses for square_1 and square_2, which were recorded at 7 and 17 s, respectively. The intensity analyses of laser images along the line L–L′ at square_1 and square_2 address the laser diffraction image change spatially. The scale bar is 100 μm. See ESI movie.†

substrate. Here we picked the nine-spot array at the center of Fresnel diffraction image for individual cell trapping. Comparing each spot in Fig. 5(a), the center spot is the brightest. The four spots next to the center spot are dimmer. The brightness of the spots at the four corners is blurred. This experimental image fits the mathematical formula (10) and the simulation results shown later in Fig. 7.

Fig. 5(a)–(d) recorded the cell trapping process into each spot at the center of the diffraction pattern in sequence within 26 s. Fig. 5(e) highlights the change of spot image identified in squares 1 and 2 of Fig. 5(b) and (c). Diffraction spots with 100 μm separation and the 15 μm spot size are shown in Fig. 5(a). The images of the laser diffraction spot projecting onto TiOPc layer and CCD plane are shown in the left of Fig. 5(e).

The laser spot, as shown in square_1, behaves like a virtual electrode on the substrate. The cell is driven toward the spot center due to the positive DEP force under the operating conditions, 5 V_{pp} (peak to peak) and 1 MHz. When the cell is trapped at the spot center, its spherical shape behaves like a lens to deflect the illuminating light path passing through the

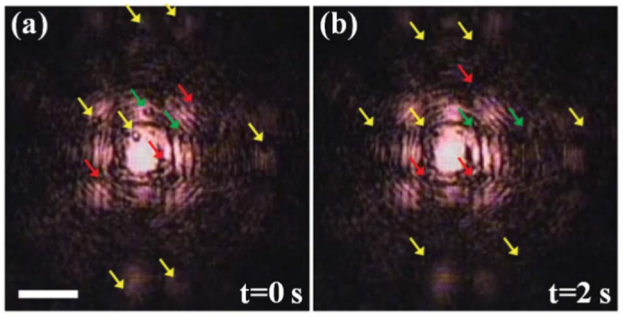

Fig. 6 The nDEP trapping gap between adjacent diffraction light spots is shortened by reducing the distance between the grid mask and the lens L1 to generate an appropriate dim region for single bead trapping. Eleven polystyrene beads are labeled with yellow, green and red arrows for tracing the position changes. With the applied ac voltage of 5 V_{pp} and 20 kHz, the nDEP forces repel the beads toward the dim nodes between each diffraction spots in 2 s. The scale bar is 100 μm. See ESI movie.†

TiOPc layer and project onto the CCD plane. Unlike the conventional cell image on an OET chip with the cell image of the clear cell circle boundary, the laser light through the spherical cell is diffracted again and projected onto the CCD plane with numerous round circles, as shown in square_2 (Fig. 5(c)). The intensity analyses of laser images along the line L–L′ at square_1 and square_2 in the right of Fig. 5(e), which show the intensity spatial changes of diffraction images projecting onto the TiOPc layer and the CCD plane. The real-time cell trapping is recorded and shown in the supplementary video, see ESI†.

Bead trapping in the dim regions

Fig. 6 shows that the 15 μm diameter polystyrene beads are moved and trapped by diffraction-induced nDEP forces. The nDEP forces repel the beads suspended in double-dilute water (DD water) from the area of diffraction illuminating toward the dim region. In the former diffraction pattern shown in Fig. 5(a), the distance between each spot is 100 μm and most of the area is dark.

According to the formula (10) for the intensity $I_Z(x_2,y_2)$ of the observed diffraction pattern, there are numerous spots formed on the TiOPc surface. The gap between each spot could be easily tuned by adjusting the relative position of the grid grating and the lenses as shown in Fig. 1 (a). If we still use the same diffraction pattern that results in Fig. 5(a) to demonstrate the nDEP trapping for polystyrene beads, the dim region is too large to form efficient traps. Therefore, we adjusted the distance z illustrated in Fig. 1(a) to tune the dim region among the diffraction spots for trapping of a single polystyrene bead. As illustrated by the schematic diagram of electric-field distribution shown in Fig. 4, the region of relatively weak electric field is between the spots which is the dim region among the laser light illumination. Because the polystyrene beads are trapped in the dim regions, it is hard to record the trapping images clearly. Therefore, yellow, red and green arrows as shown in Fig. 6 are used to identify/trace each bead before and after light-induced nDEP forces are applied. When the ac potential of 5 V_{pp} at 20 kHz is applied to the chip, the nDEP forces immediately drive the beads toward the dim region between each illuminating spot. HepG2 cells are trapped on the bright spots and polystyrene beads are repelled toward the dim region of the laser diffraction pattern shown in Fig. 6 and Fig. 7, respectively.

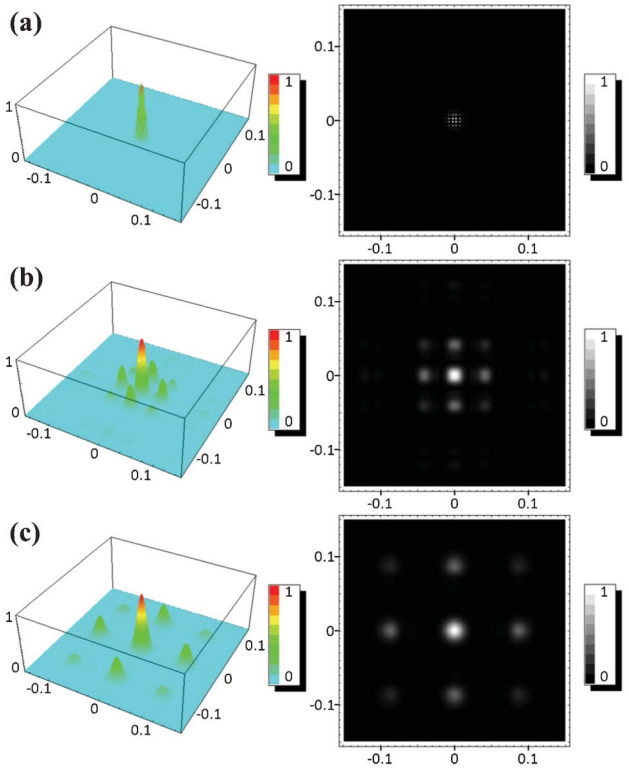

Fig. 7 The simulation results for corresponding Fresnel diffraction images using Mathematica 7 software. Distribution of the laser diffraction spots can be tuned by adjusting the relative position of the grid-shape grating mask, lenses, and TiOPc surface. (a), (b) and (c) show the simulation results of diffraction pattern on the TiOPc layer under the conditions z = 0 mm, 250 mm, and 550 mm (Fig. 1(a)), respectively.

Fresnel diffraction simulation

The grating pattern mask which consists of a 100 μm × 100 μm hollow square aperture array and a 100 μm gap is shown in Fig. 1 (b). One coherent laser beam passes through a grid grating to generate an optical diffraction pattern, which forms the Fresnel diffraction of wave propagation. Mathematica 7 software (Wolfram Co., Ltd.) was utilized to simulate the intensity of the diffraction pattern and to investigate the diffraction pattern projected onto the TiOPc surface.

The dispersed pattern through the grating mask is focused on the focal plane of the lens L2 as shown in Fig. 1(a). The TiOPc chip surface is placed on the focal plane of the lens L2. A perfect focusing pattern as simulated and shown in Fig. 7(a) could be formed. However, the spot size and the gap are too small to trap microparticles. In order to generate appropriate trapping spots with the right size to confine the target cells and polystyrene beads, we adjusted the distance z between the mask and the lens L1 (Fig. 1(a)). When the z value is tuned, the diameter size of each spot at (x_2, y_2) plane could be increased

and the spots' size on the TiOPc surface could be also enlarged.

In our experiments, the appropriate z distance was chosen for fitting our microscope's field of view, 1 mm × 1 mm, to demonstrate the light-induced DEP phenomena clearly. The larger illuminating region or the specific spot separation gap/pattern can be achieved by tuning the parameters of the optical system and redesigning the grating mask. Fig. 7(b) shows the simulation result for the Fresnel diffraction image with the brighter nine spots on the TiOPc surface with the z value of 250 mm. The image with a small dim region between each spot was applied to trap single polystyrene bead. Fig. 7(c) shows the simulation result for the z value of 550 mm. We utilized this pattern to trap HepG2 cells with pDEP forces.

The average power density of the incident laser on the diffraction grating was 177 mW cm^{-2} generated by a 0.5 mW He–Ne laser with a 0.6 mm beam diameter. According to the simulation results, the maximum power density on the photoconductive substrate is less than 3.48 W cm^{-2} when the loss of the optical system is neglected and z = 550 mm. This power density, larger than 0.33 mW cm^{-2}, has enough energy to change the impedance of the TiOPc layer and to generate the DEP phenomenon.[41] In addition, the power density of the diffraction primary spot is too small to generate either a dominant temperature rises or a dominant electrothermal (ET) flow effect. The applied frequency, 1 MHz, is also not low enough to induce ac electroosmosis flow on the TiOPc surface.[41,42] Therefore, the light-induced DEP phenomenon predominates under our operating conditions.

Operation conditions for cellular applications

We used TiOPc as the photoconductive material to fabricate an OET chip in our research developments. When compared with the reported thickness of a-Si based photoconductive layer, 1–2 μm,[16,43,44] our TiOPc layer of 200 nm is thinner. The illuminating power density of 0.33 mW cm^{-2} within 700–800 nm wavelength is enough to generate the DEP phenomenon on our TiOPc-based chip.[41] The thinner layer on our chip reduces the absorption of the illuminating power and reduces the temperature rises due to joule heating.[41] However, the a-Si layer is durable in common organic solvents, however the liquid solution containing either alcohol or acetone could erase the TiOPc coating. It also means that the TiOPc coating layer cannot endure standard photolithography with acetone wash step to fabricate specific microchannel on the TiOPc surface. The microchannels fabricated on the light-induced DEP platform could bring the convenience of liquid handling.[38,45] Although using a PEGDA-based microchannel already could provide a method to guide liquid flow direction on the TiOPc-coating surface,[46] it has the potential advantages to further combine TiOPc-based devices and microfluidics for further applications.

The applied voltage, ac frequency, and sandwiched medium are three important factors for the operation of our TiOPc-based chips. By using a function generator and power supply, we tested our TiOPc chip by tuning the applied potential of 0–10 V_{pp} and 1–20 MHz. Based on the OET operation principle, the sandwiched medium could affect the OET operating ranges of applied voltage and frequency. For example, most of the voltage drops across the low electric-conductivity medium such as silicone oil and the TiOPc layer is durable under the conditions of 10 V_{pp} ac voltage from 1 Hz to 20 MHz to drive 60 μm diameter gas bubbles.[41] When the sandwiched medium has a relatively high conductivity such as an aqueous solution, deionized water, phosphate buffered saline (PBS) buffer, and cell culture medium, most of the voltage drops across the 200 nm-thickness TiOPc layer. Then, the TiOPc property deteriorates under the operating conditions of 7–10 V_{pp} at 10 kHz. The electrolytic bubble generated under the low ac frequency and high voltage tends to damage the TiOPc layer. If the operating conditions are selected and tuned carefully, within the low ac frequency and the low voltage region, to avoid electrolysis, it is possible to observe light-induced ac electroosmosis (LACE) phenomenon.[42,47–49] LACE is caused by the light-induced tangential electric field. Briefly, ac electroosmosis and the LACE effect are the surface flow driven by the ions' movement on the electrical double layer (EDL).They are both frequency dependent.[42] The light-induced electroosmosis flow has been reported to concentrate 2 μm diameter magnetic beads with the illuminating light pattern on the TiOPc-based chip under the low ac frequency/voltage operating conditions.[50] Therefore, choosing appropriate operating conditions of ac voltage and frequency according to the sandwiched medium can maintain the TiOPc layer property and cause the corresponding phenomenon. The information regarding these operating conditions and the corresponding phenomenon on the TiOPc-based chip are summarized in Table 1.

For biological applications such as cell manipulation, the operating conditions of voltage and frequency are needed to be chosen carefully. Studies for the appropriate voltage to manipulate cells for electroporation on a light-induced optoelectronic platform have been reported.[51] Briefly, the cell membrane is perforated when the electric field is above about 1.4 kV cm^{-1}. The membrane structure is reversible until the electric-field strength reaches approximately 2.3 kV cm^{-1}. For our TiOPc chip, the gap between the top ITO glass and the bottom TiOPc substrate is defined by tapes, about 80–200 um. Under 3–5 Vpp ac voltage, the maximum electric-field strength

Table 1 The operating conditions and corresponding phenomenon on the TiOPc-based chip

Particle & medium	Operating principle	Voltage (V_{pp})	Frequency (Hz)
HepG2 Cell & DEP buffer[28]	DEP	3–5	>1 M
Gas bubble & silicone oil[41]	DEP	0–10	1–20 M
PS bead & DD water[28]	DEP	7	20 k
Magnetic bead & DD water[50]	LACE	5	10 k

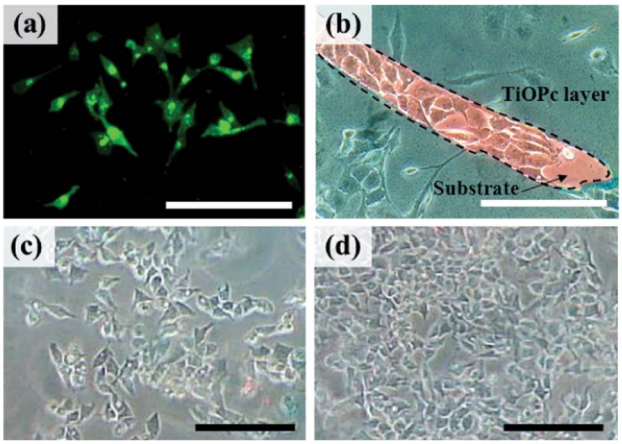

Fig. 8 HepG2 cells morphology after 12 h, 24 h, 48 h, and 72 h of culture on the TiOPc-coating surface. (a) Cells started to adhere and spread on TiOPc-coating surface after 12 h of culture. (b) The cells in both regions, the TiOPc-coating surface and the scraped glass surface, have similar cell behaviour and morphology after 24 h of culture. (c) and (d) The growth and morphology of the cells on the TiOPc-coating surface after 48 h and 72 h of culture. The number of HepG2 cells increases after 48 h of culture. The cells cover about 80% of the TiOPc-coating surface after 72 h. The scale bar is 100 μm.

is estimated to be about 0.6 kV cm^{-1}.[52] This electric-field strength is not strong enough to perforate the cell membrane and to result in dominant temperature rises.[42,45] In addition to the voltage and frequency, the conductivity of the medium should also be considered for the sake of cell viability and DEP operation.[53] A normal biological buffer with a high electrical conductivity has two limitations for the cell DEP manipulation, joule heating of the solution and electrolysis in low ac frequency. Therefore, a low conductivity medium for the cell DEP manipulation could decrease the field-induced apoptosis. Cell reactions under DEP operating conditions in a low conductivity medium have ever been reported by our group. The 95% cell viability is assayed under the operating condition of 5 V_{pp} and 1 MHz in the buffer conductivity of 10 mS m^{-1}.[7,54]

TiOPc has been widely used and coated on a photoconductor drum for laser printing. Studies of its biocompatibility will provide valuable evidence for the relative biological applications. In order to observe the basic cell reactions responding to TiOPc, HepG2 cells were seeded on the TiOPc-coating surface, placed into a CO_2 incubator and cultured under the standard cells culture conditions. Their morphology was observed after 12 h, 24 h, 48 h, and 72 h of culture and are shown in Fig. 8. After 12 h of culture, the HepG2 cells adhered onto the TiOPc surface and showed a morphological change, spreading their shape, Fig. 8(a). We scraped a small part of the TiOPc layer to observe the cell morphology on the TiOPc rough surface and the smooth glass surface. The cells in both regions had similar cell behaviour and morphology after 24 h of culture (Fig. 8(b)). The cells' growth confined within the glass region was observed. The height difference between the glass surface and the TiOPc layer is 200 nm. After 48 h and 72 h of culture, the cell number increased (Fig. 8(c) and (d)) to cover about 80% surface area for 72 h of culture. According to the observation of cell morphological changes within 5 days, the HepG2 cells cultured on TiOPc surface showed similar growth speed and behaviour to those cultured on normal cell culture dish.

Although the TiOPc-coating surface is still able to demonstrate the DEP phenomenon after several months and the dried layer is not dissolved in aqueous solution,[28] it is not recommended to replace the normal cell dish with the TiOPc-coating substrate for long-time cell culture after the DEP operation due to the less experimental data being available to prove its long-term biocompatibility. The feature of TiOPc material is to facilitate DEP/OET phenomena for real-time cell manipulation, however the cells viability would be decreased under the conditions of high voltage treatment, low-nutrition culture medium, and low conductivity DEP sugar buffer over 2 h.

Since optoelectronic manipulation (OET) was presented in 2005, various developments of this platform have attracted much research to explore its capability. A-Si-based substrates still form the majority of chip materials until now.[23,44,55] Here, we discuss the advantages and limitations of organic TiOPc compared with a-Si as related to the materials' applications. From the point of view for chip fabrication, TiOPc is more convenient, cost saving, and thinner than an a-Si layer. There are two advantages of the thinner TiOPc stucture, avoiding the temperature rises resulting from absorbing joule heating and decreasing the required light power density. Similar to 1 μm a-Si layer, the 200 nm TiOPc thickness can also prevent tunneling charges passing through it. The conductivity of both TiOPc and a-Si layers can be increased by light illumination. However, the thinner TiOPc layer cannot endure washing with an aqueous alcohol solution. Less resistance for high-voltage and low-frequency operating conditions, such as light-induced ac electroosmosis and electrothermal flow phenomenon, could be the limitation for the TiOPc material.

Conclusions

In this research we converted a single He–Ne laser beam into the diffraction image with a grid-shape grating mask consisting of a 100 μm × 100 μm square aperture array. This diffraction pattern induced a multi-spot array of virtual electrodes on the TiOPc-based optoelectronic chip and generated a non-uniform electric field to pattern HepG2 cells and polystyrene beads with positive/negative DEP forces. For the analyses of the wave propagation and the microparticle manipulation, Fresnel diffraction and the DEP principle were simulated to study the experimental results, the power density of diffraction pattern and the electric-field distribution induced by virtual electrode spots. Additionally, some discussions and comparisons of TiOPc-based and a-Si-based OETs were addressed in this paper. Furthermore, the 5-day observation of HepG2 morphology changes also demonstrates that the HepG2 cells experienced TiOPc-based OET manipulation and, cultured on TiOPc surface, showed similar growth speed and behaviour to those cultured on a normal cell culture dish. Because of the various potential biological applications, more biocompatibility assays for the cells on the TiOPc material are

worthy of further investigation. In this paper, we demonstrated cell/bead patterning/trapping *via* diffraction-induced optoelectronic dielectrophoresis force on our TiOPc-based photoconductive chip.

Acknowledgements

This project was financially sponsored by the National Science Council (Grant No.98-2120-M-007-003). We extend special thanks to Prof. Ming C. Wu at University of California, Berkeley and Prof. Pei-Yu Chiou at University of California, Los Angeles for the knowledge sharing of optoelectronic technology. We acknowledge Prof. Hwan-You Chang and the group member in his Microbiology and Biotechnology Laboratory at National Tsing Hua University for biological supports. We also thank Dr Ming-Huei Liu and the Sinonar Corp. (Hsinchu, R.O.C.) for the photoconductivity material support.

References

1 T. G. Fernandes, *et al.*, Three-dimensional cell culture microarray for high-throughput studies of stem cell fate, *Biotechnol. Bioeng.*, 2010, **106**(1), 106–118.
2 D. B. Wheeler, A. E. Carpenter and D. M. Sabatini, Cell microarrays and RNA interference chip away at gene function, *Nat. Genet.*, 2005, **37**, S25–S30.
3 C. J. Flaim, S. Chien and S. N. Bhatia, An extracellular matrix microarray for probing cellular differentiation, *Nat. Methods*, 2005, **2**(2), 119–125.
4 D. Qin, Y. Xia and G. M. Whitesides, Soft lithography for micro- and nanoscale patterning, *Nat. Protoc.*, 2010, **5**(3), 491–502.
5 S. R. Khetani and S. N. Bhatia, Microscale culture of human liver cells for drug development, *Nat. Biotechnol.*, 2008, **26**(1), 120–126.
6 STEVENS, *et al.*, *Direct patterning of mammalian cells onto porous tissue engineering substrates using agarose stamps*, Vol. 26, 2005, Oxford, ROYAUME-UNI, Elsevier, p. 6.
7 C.-T. Ho, *et al.*, Rapid heterogeneous liver-cell on-chip patterning via the enhanced field-induced dielectrophoresis trap, *Lab Chip*, 2006, **6**(6), 724–734.
8 C. Smith, Tools for drug discovery: Tools of the trade, *Nature*, 2007, **446**(7132), 219–222.
9 A. Ashkin, J. M. Dziedzic and T. Yamane, Optical trapping and manipulation of single cells using infrared laser beams, *Nature*, 1987, **330**(6150), 769–771.
10 K. C. Neuman and S. M. Block, Optical trapping, *Rev. Sci. Instrum.*, 2004, **75**(9), 2787–2809.
11 E. R. Dufresne and D. G. Grier, Optical tweezer arrays and optical substrates created with diffractive optics, *Rev. Sci. Instrum.*, 1998, **69**(5), 1974–1977.
12 B. Sun, Y. Roichman and D. G. Grier, Theory of holographic optical trapping, *Opt. Express*, 2008, **16**(20), 15765–15776.
13 R. Pethig, Review Article-Dielectrophoresis: Status of the theory, technology, and applications, *Biomicrofluidics*, 2010, **4**(2), 022811–35.
14 C. Zhang, *et al.*, Dielectrophoresis for manipulation of micro/nano particles in microfluidic systems, *Anal. Bioanal. Chem.*, 2010, **396**(1), 401–420.
15 B. H. Lapizco-Encinas and M. Rito-Palomares, Dielectrophoresis for the manipulation of nanobioparticles, *Electrophoresis*, 2007, **28**(24), 4521–4538.
16 P. Y. Chiou, A. T. Ohta and M. C. Wu, Massively parallel manipulation of single cells and microparticles using optical images, *Nature*, 2005, **436**(7049), 370–372.
17 J. K. Valley, *et al.*, A unified platform for optoelectrowetting and optoelectronic tweezers, *Lab Chip*, 2011, **11**(7), 1292–1297.
18 Y.-S. Lu, *et al.*, Controllability of Non-Contact Cell Manipulation by Image Dielectrophoresis (iDEP), *Opt. Quantum Electron.*, 2005, **37**(13), 1385–1395.
19 H.-Y. Hsu, *et al.*, Phototransistor-based optoelectronic tweezers for dynamic cell manipulation in cell culture media, *Lab Chip*, 2010, **10**(2), 165–172.
20 A. T. Ohta, *et al.*, Dynamic Cell and Microparticle Control via Optoelectronic Tweezers, *J. Microelectromech. Syst.*, 2007, **16**(3), 491–499.
21 A. T. Ohta, *et al.*, Optically Controlled Cell Discrimination and Trapping Using Optoelectronic Tweezers, *IEEE J. Sel. Top. Quantum Electron.*, 2007, **13**(2), 235–243.
22 W. Choi, *et al.*, Programmable manipulation of motile cells in optoelectronic tweezers using a grayscale image, *Appl. Phys. Lett.*, 2008, **93**(14), 143901–3.
23 M. C. Wu, Optoelectronic tweezers, *Nat. Photonics*, 2011, **5**(6), 322–324.
24 G. Haulot, A. J. Benahmed and C.-M. Ho, Optoelectronic reconfigurable microchannels, *Lab Chip*, 2012, **12**(23), 5086–5092.
25 J. Moffitt, *et al.*, Recent Advances in Optical Tweezers, *Annu. Rev. Biochem.*, 2008, **77**(1), 205–228.
26 D. G. Grier, A revolution in optical manipulation, *Nature*, 2003, **424**(6950), 810–816.
27 W. Wang, *et al.*, Bulk-heterojunction polymers in optically-induced dielectrophoretic devices for the manipulation of microparticles, *Opt. Express*, 2009, **17**(20), 17603–17613.
28 S. M. Yang, *et al.*, Dynamic manipulation and patterning of microparticles and cells by using TiOPc-based optoelectronic dielectrophoresis, *Opt. Lett.*, 2010, **35**(12), 1959–1961.
29 K. Y. Law, Organic photoconductive materials: Recent trends and developments, *Chem. Rev.*, 1993, **93**(1), 449–486.
30 C. J. Lee, J. H. Park and J. Park, Synthesis of bamboo-shaped multiwalled carbon nanotubes using thermal chemical vapor deposition, *Chem. Phys. Lett.*, 2000, **323**(5–6), 560–565.
31 K. Ogawa, *et al.*, Chemical behaviour of oxotitanium(IV) phthalocyanine (OTiPc) solutions associated with the preparation of OTiPC monolayers and multilayers, *J. Mater. Chem.*, 1996, **6**(2), 143–147.
32 S. Yamaguchi and Y. Sasaki, Primary carrier-generation process in Y-form and phase I titanyl phthalocyanines, *Chem. Phys. Lett.*, 2000, **323**(1–2), 35–42.
33 W.-B. Wang, *et al.*, The preparation of high photosensitive TiOPc, *Dyes Pigm.*, 2007, **72**(1), 38–41.
34 K. F. Hoettges, Dielectrophoresis as a Cell., *Characterisation Tool.*, 2008, 183–198.
35 A. Jamshidi, *et al.*, Dynamic manipulation and separation of individual semiconducting and metallic nanowires, *Nat. Photonics*, 2008, **2**(2), 86–89.

36 H. Hwang, *et al.*, Interactive manipulation of blood cells using a lens-integrated liquid crystal display based optoelectronic tweezers system, *Electrophoresis*, 2008, **29**(6), 1203–1212.
37 J. K. Valley, *et al.*, Optoelectronic Tweezers for quantitative assessment of embryo developmental stage, in, *Micro Electro Mechanical Systems (MEMS), 2010 IEEE 23rd International Conference on*, 2010.
38 Y.-H. Lin and G.-B. Lee, Optically induced flow cytometry for continuous microparticle counting and sorting, *Biosens. Bioelectron.*, 2008, **24**(4), 572–578.
39 H. Hwang, *et al.*, Reduction of nonspecific surface-particle interactions in optoelectronic tweezers, *Appl. Phys. Lett.*, 2008, **92**(2), 024108–024108-3.
40 H. Hwang and J.-K. Park, Rapid and selective concentration of microparticles in an optoelectrofluidic platform, *Lab Chip*, 2009, **9**(2), 199–206.
41 S.-M. Yang, *et al.*, Light-driven manipulation of picobubbles on a titanium oxide phthalocyanine-based optoelectronic chip, *Appl. Phys. Lett.*, 2011, **98**(15), 153512–3.
42 J. K. Valley, *et al.*, Operational Regimes and Physics Present in Optoelectronic Tweezers, *J. Microelectromech. Syst.*, 2008, **17**(2), 342–350.
43 W. Choi, *et al.*, Lab-on-a-display: a new microparticle manipulation platform using a liquid crystal display (LCD), *Microfluid. Nanofluid.*, 2007, **3**(2), 217–225.
44 H. Hwang and J.-K. Park, Optoelectrofluidic platforms for chemistry and biology, *Lab Chip*, 2011, **11**(1), 33–47.
45 J. K. Valley, *et al.*, Parallel single-cell light-induced electroporation and dielectrophoretic manipulation, *Lab Chip*, 2009, **9**(12), 1714–1720.
46 S.-M. Yang, *et al.*, Moldless PEGDA-Based Optoelectrofluidic Platform for Microparticle Selection, *Adv. OptoElectron.*, 2011, **2011**, 8.
47 A. Jamshidi, *et al.*, NanoPen: Dynamic, Low-Power, and Light-Actuated Patterning of Nanoparticles, *Nano Lett.*, 2009, **9**(8), 2921–2925.
48 S. Lee, *et al.*, Optoelectrofluidic field separation based on light-intensity gradients, *Biomicrofluidics*, 2010, **4**(3), 034102.
49 C. Pei-Yu, *et al.*, Light-Actuated AC Electroosmosis for Nanoparticle Manipulation, *J. Microelectromech. Syst.*, 2008, **17**(3), 525–531.
50 Y. Shih-Mo, *et al.*, Concentration of Magnetic Beads Utilizing Light-Induced Electro-Osmosis Flow, *IEEE Trans. Magn.*, 2011, **47**(10), 2418–2421.
51 J. K. Valley, *et al.*, Parallel single-cell light-induced electroporation and dielectrophoretic manipulation, *Lab Chip*, 2009, **9**(12), 1714–1720.
52 P. R. C. Gascoyne and J. V. Vykoukal, Dielectrophoresis-based sample handling in general-purpose programmable diagnostic instruments, *Proc. IEEE*, 2004, **92**(1), 22–42.
53 Z. Yu, *et al.*, Negative Dielectrophoretic Force Assisted Construction of Ordered Neuronal Networks on Cell Positioning Bioelectronic Chips, *Biomed. Microdevices*, 2004, **6**(4), 311–324.
54 C.-T. Ho, *et al.*, Liver-cell patterning Lab Chip: mimicking the morphology of liver lobule tissue, *Lab on a Chip*, 2013, DOI: 10.1039/C3LC50402F.
55 A. Kumar, *et al.*, Hybrid opto-electric manipulation in microfluidics-opportunities and challenges, *Lab Chip*, 2011, **11**(13), 2135–2148.

